JOURNAL OF AIRCRAFT
Vol. 47, No. 6, November–December 2010

Small and Micro Aerial Vehicles: How Much Span is Too Much Span?

Götz Bramesfeld*
Saint Louis University, St. Louis, Missouri 63103

DOI: 10.2514/1.C000238

This paper explores at what point a further span increase, while maintaining a constant wing area and loading, results in a reduction in aerodynamic performance. Especially in the case of small and micro aerial vehicles, a span increase can be realized with only a minor weight penalty. Of particular interest are the maximum lift-to-drag ratio and the minimum power required. The existence of such extrema with respect to the aspect ratio is based on the notion that, while increasing the span decreases the induced drag, it also increases the profile drag as a result of the decreasing chord Reynolds number. The increasing profile drag eventually leads to a performance loss despite the growing aspect ratio. This behavior is investigated using an analytical and a computational approach. Whereas the analytical approach does not reveal distinct limits in beneficial aspect ratios, the computational approach indicates the existence of such limits, especially for lower flight masses below 500 g. The computations suggest, for a 100 g wing with fixed span, that doubling the aspect ratio from one to two results in a 20% endurance increase.

Nomenclature

AR	=	aspect ratio, b^2/S
b	=	wingspan
C_D	=	three-dimensional drag coefficient
$C_{D,se}$	=	wing-tip suction drag coefficient
C_{Di}	=	induced drag coefficient
C_{Dp}	=	wing-profile drag coefficient
C_{D0}	=	zero-lift drag coefficient of wing
C_L	=	lift coefficient
$\hat{C}_L$	=	lift coefficient of maximum lift-to-drag ratio
$\tilde{C}_L$	=	lift coefficient of minimum power required
c	=	wing chord
c_d	=	section drag coefficient
D	=	drag force
D_i	=	induced drag
D_p	=	profile-drag force
e	=	span efficiency, $C_{\mathrm{Dind}}/C_{\mathrm{Dind,elliptical}}$
$K_{v,se}$	=	wing-tip suction force coefficient
k_1–k_4	=	general constants
L	=	lift force
L/D	=	lift-to-drag ratio
P	=	power required
q	=	dynamic pressure
Re	=	chord Reynolds number, $V_\infty c/\nu$
S	=	wing area
V_{eq}	=	equivalent airspeed
V_∞	=	freestream airspeed
W	=	aircraft weight
α	=	angle of attack
ν	=	kinematic viscosity
ρ	=	air density

Introduction

IN GENERAL, increasing the wingspan of an aircraft is a relatively simple way to improve its flight performance. If no structural or other penalties occur due to the large span, the subsequent lower-span loading results in a reduction in induced drag and, thus, the total drag. This favorably influences the maximum lift-to-drag coefficient, $(C_L/C_D)_{\max}$, as well as the nondimensional minimum power-required condition, $(C_L^{1.5}/C_D)_{\max}$, two design points that correspond with maximum range and maximum endurance of propeller-driven aircraft, respectively.

Nevertheless, structural and ground handling restrictions can put limits on the possibility to improve the flight performance using a simple wingspan increase. A larger wingspan typically increases the root-bending moment and the likelihood of aeroelastic issues so that some combination of complexity and weight must be added to the wing structure. The subsequent weight increases may offset any gains in flight performance. In addition, large spans can overly complicate ground handling, for example, due to the restricted width of a given taxiway or runway. Further limitations are associated with the launch and recovery method employed, for instance, if done by hand, as it is often the case with small uninhabited aerial vehicles. Overall, issues other than purely aerodynamic performance can become the limiting factors in any wingspan decision.

The structural limitations due to larger aspect ratios are of much lesser concern for the design of small uninhabited and micro aerial vehicles (MAVs) than for larger, conventional aircraft [1]. Especially modern composite materials permit high aspect-ratio structures that are still well suited for the expected flight loads of these vehicles. Nevertheless, many recent MAV designs appear to prefer smaller aspect ratios that are near unity [2–5]. The decision for such low aspect ratios is driven by other than purely aerodynamic performance considerations. For example, a low aspect ratio will maximize the wing area and, thus, minimize stall speed if the maximum aircraft dimensions are limited due to storage or other restrictions, such as a confined operational space inside a building. In addition, low aspect-ratio wings may take advantage of vortical effects, such as lift due to leading-edge and side-edge separation. These vortical effects may further reduce the stall speed and aid launch and recovery efforts [6–8]. Nevertheless, such aerial vehicles are severely constrained in range and endurance due to their limitation of propellant volume and the weight that they can carry. Thus, in order to maximize range and/or endurance, the designs of small uninhabited vehicles and MAVs require a high aerodynamic efficiency that, as for any aircraft, is greatly affected by the induced drag and parasitic, primarily profile drag. For small vehicles and MAVs, however, the profile drag is strongly impacted by low Reynolds number flow and, thus, can significantly exceed the induced drag over the entire flight range. Only relatively small changes in the chord Reynolds number, for example, due to a variation in aspect ratio, can cause significant

Received 29 December 2009; revision received 18 April 2010; accepted for publication 21 June 2010.

*Assistant Professor, Department of Aerospace and Mechanical Engineering and Center for Fluids at All Scales. Member AIAA.

viscous drag changes with subsequent changes in overall aerodynamic efficiency. This leads to the central question regarding at what aspect ratio the performance gains of the lower induced drag of the larger span are outweighed by the cost of the higher profile drag due to the lower chord. In other words, what is the aspect ratio that ultimately maximizes the overall flight performance of small vehicles and MAVs?

In a parametric study of very lightweight wings, the lift-to-drag ratios display distinct maxima with varying aspect ratios, as shown in Fig. 1 [1]. In that study, the aspect ratios were varied by changing the wing chord while maintaining a constant lift, wingspan, span efficiency, and airspeed. Thus, the different aspect ratios have identical induced drags, and the study solely captures the profile drag changes due to the variations in wing-area and profile-drag coefficients that are a function of the chord Reynolds numbers. Already at moderate aspect ratios, the increases in profile-drag coefficients outweigh the gains in wing area reduction and result in performance degradations at higher aspect ratios.

In addition to the Reynolds number effects, the possible reduction in span efficiency of the larger wingspan, as shown in Fig. 2, compound the notion of a performance-maximizing aspect ratio. In the case of a rectangular wing without twist and relatively independent of lift coefficient, the span efficiency of a rectangular wing peaks at an aspect ratio of four and drops notably for smaller and larger aspect ratios. The unfavorable developments in the span efficiency of the smaller and larger aspect ratios are due to strong roll-up effects of the wake and spanwise lift distributions that deviate significantly from an elliptical, respectively. Although the span efficiency can be raised using twist and/or the appropriate planform choice, these gains come at the cost of a higher complexity of the wing design.

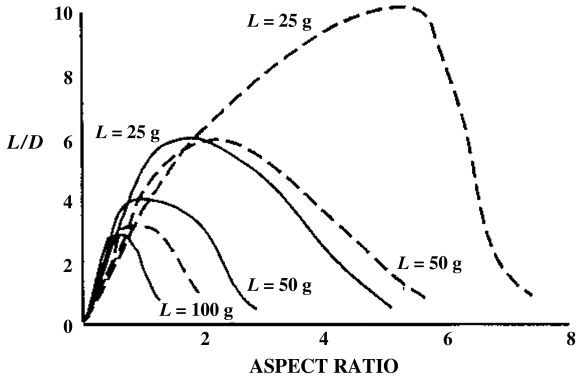

Fig. 1 Results of a parametric study of varying wing chords at a constant span of 300 mm, an airspeed of 5 m/s, and a span efficiency of 0.8 [1]. The solid lines represent the results using a flat-plate airfoil, and the dashed lines represent that of a thin cambered plate.

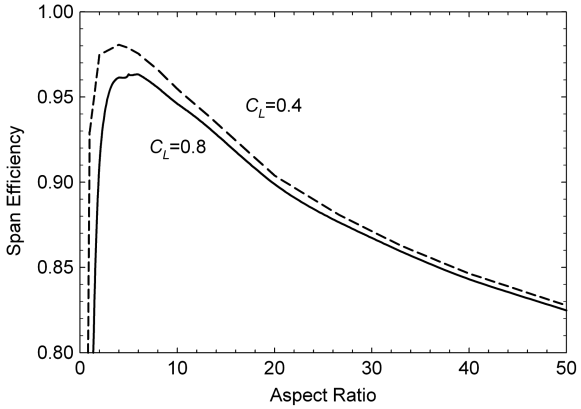

Fig. 2 Theoretical span efficiencies versus the aspect ratio of a rectangular wing without twist. The computational results are based on a model using a relaxed force-free wake [13].

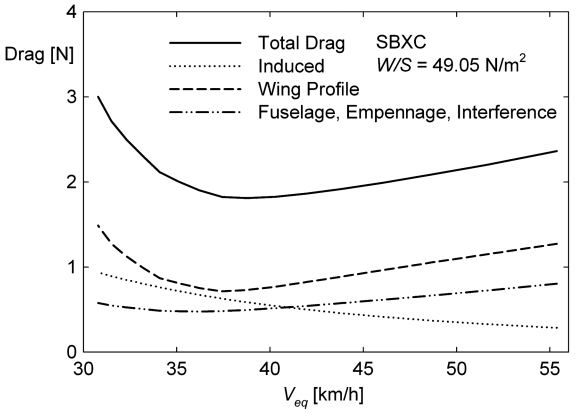

Fig. 3 Drag decomposition of a small uninhabited aerial vehicle with a wing area 1 m^2 of aspect ratio 18.9. The wing profile is the S2048 airfoil.

This paper tries to explore this optimal aspect ratio. The optimal aspect ratio is considered to be the one that maximizes the flight performance of a given flight weight. The performance parameters of interest are the minimum power required and the maximum lift-to-drag ratio. Of particular interest are the effects that are associated with the aerodynamics of small vehicles and MAVs. Their low Reynolds number operating range provides interesting trade studies. For example, whereas the classical drag approach [9,10] assumes that the maximum lift-to-drag ratio is signified by induced and parasite drag being of equal magnitude, in the case of small vehicles and MAVs, the parasitic drag can be considerably larger than the induced drag over the entire flight envelope due to the rather larger profile drags of the low Reynolds number airfoils, as illustrated in Fig. 3, with the drag decomposition of a small uninhabited aerial vehicle. The wing profile drag of that particular aircraft consistently exceeds the induced drag as the Reynolds number, based on the average wing chord length, varies from approximately 150,000 to 270,000.

This paper has three main parts. In the section titled Analytical Approach to the Optimal Aspect Ratio, an analytical approach is used to explore what aspect ratios maximize the lift-to-drag ratio and minimize the power required for a given wing area and weight. This analysis makes use of an analogy of the nearly logarithmic behavior of the flat-plate drag coefficient. A computational investigation of the optimal aspect ratio is discussed in the section titled Quantitative Evaluation of the Optimal Aspect Ratio. Although the results presented herein are primarily focused on the analysis of the performances of wings, the influence of secondary effects, such additional drag penalties due a fuselage or trim, are also discussed. In the section titled Conceptual Design Examples Based on the Optimal Aspect Ratio, the numerical results of the section titled Quantitative Evaluation of the Optimal Aspect Ratio are used to demonstrate the potential performance benefits of an optimized aspect ratio, using two case studies of conceptual designs examples of a 2 kg unmanned aerial vehicle (UAV) and a 100 g MAV.

Analytical Approach to the Optimal Aspect Ratio

The question remains about if an optimal aspect ratio exists and what it is. In this section, an analytical approach is chosen to explore the question of an optimal aspect ratio at which the lift-to-drag ratio and minimum power required reach their maximum limit. For the analysis, it is necessary to express the total wing drag in terms of lift coefficient and aspect ratio. The drag contribution of the induced effects is relatively easily expressed as a function of the lift coefficient and aspect ratio:

$$C_{Di} = k_1 \frac{C_L^2}{\mathrm{AR}} \tag{1}$$

where $k_1 = 1/(e\pi)$. The span-efficiency factor e depends on the spanwise lift distribution and is unity in the case of an elliptical lift distribution. The viscous effects of the wing drag are approximated

using a profile-drag coefficient that is constant across the span and always at a minimum, thus independent of the angle of attack. This minimum profile-drag coefficient depends on the chord Reynolds number and is approximated using a power relationship:

$$C_{Dp} = k_2 Re^{k_3} \tag{2}$$

Examples of such relationships are plotted in Fig. 4. In the case of a flat plate that has laminar boundary layers on both sides, the constants are $k_2 = 2 \cdot 1.328$ [9] and $k_3 = -0.5$. The constants of the turbulent flat plate are $k_2 = 2 \cdot 0.074$ [9] and $k_3 = -0.2$. It should be noted that the boundary layer of a flat plate is predominately laminar at Reynolds numbers below 50,000. In addition to the flat-plate drags, the minimum drag coefficients of the NACA 0009 airfoil were computed using XFOIL [11] and are also plotted in Fig. 4. Below $Re < 10^6$, the subsequent constants are $k_2 = 2.772$ and $k_3 = -0.47$. The k_3 exponent is very similar in value to the one of a laminar flat plate, suggesting that the low Reynolds number flow is primarily dictated by a laminar boundary layer. These theoretical results, however, have to be considered with caution, since at these very low Reynolds numbers, some of the assumptions made in the airfoil analysis do not apply any longer, such as the assumption that the effects of the viscous boundary layer remain restricted to a relatively small range. Nevertheless, in lieu of better available data, the XFOIL predictions are used in the herein-presented analysis.

To express the profile-drag coefficient of Eq. (2) in terms of lift coefficient and aspect ratio, the following relationships for chord and freestream velocity are used:

$$c = \sqrt{\frac{S}{\mathrm{AR}}} \quad \text{and} \quad V_\infty = \sqrt{\frac{2W}{\rho S C_L}}$$

which yield, for the Reynolds number, in terms of lift coefficient and aspect ratio,

$$Re = \frac{V_\infty c}{\nu} = \frac{1}{\nu}\sqrt{\frac{2W}{\rho C_L \mathrm{AR}}} \tag{3}$$

Substituting this relationship into Eq. (2) yields a function of the profile-drag coefficient with only the lift coefficient and aspect ratio as variables:

$$C_{Dp} = k_2 \left(\frac{1}{\nu}\sqrt{\frac{2W}{\rho}}\right)^{k_3} (C_L \mathrm{AR})^{k_4} \tag{4}$$

with

$$k_4 = -\frac{1}{2} k_3 \tag{5}$$

It should be noted that, in general, the constants $k_3 < 0$ and $k_4 > 0$ and, thus, the profile-drag coefficient in Eq. (4) are proportional to the lift coefficient, which reflects the inverse proportionality between the Reynolds number and the drag: the higher the lift coefficient, the lower the airspeed, and the lower the Reynolds number, the higher the drag coefficient.

The total drag coefficient of the wing can be expressed in terms of lift coefficient and aspect ratio using Eqs. (1) and (4):

$$C_D = C_{Di} + C_{Dp}; \qquad C_D = k_1 \frac{C_L^2}{\mathrm{AR}} + k_2 \left(\frac{1}{\nu}\sqrt{\frac{2W}{\rho}}\right)^{k_3} (C_L \mathrm{AR})^{K_4} \tag{6}$$

The expression in Eq. (6) can be used to analytically determine the maximum lift-to-drag ratio, C_L/C_D, and the minimum power-required point, $C_L^{1.5}/C_D$. This drag equation is very similar to the parabolic drag polar frequently used in text books to describe the performance of aircraft, for example, [9,10]. In theses cases, however, the parasitic drag term is independent of the Reynolds number effects, an acceptable assumption at higher Reynolds numbers. Nonetheless, at lower Reynolds numbers, such effects need to be considered.

Maximum Lift-to-Drag Ratio

Based on Eq. (6), the lift-to-drag ratio stated in terms of lift coefficient and aspect ratio is

$$\frac{L}{D} = \frac{C_L}{C_D} = \frac{C_L}{k_1 (C_L^2/\mathrm{AR}) + k_2 [(1/\nu)\sqrt{(2W/\rho)}]^{k_3} (C_L \mathrm{AR})^{K_4}} \tag{7}$$

The maximum lift-to-drag ratio can be found using the derivative of Eq. (7) with respect to the lift coefficient. The subsequent result yields for the maximum lift-to-drag ratio:

$$\left(\frac{L}{D}\right)_{\max} = \frac{2}{4 + k_3} \left\{ \frac{\mathrm{AR}^{1+k_3}}{k_2 [(1/\nu)\sqrt{(2W/\rho)}]^{k_3}} \times \left[\pi e \left(1 + \frac{k_3}{2}\right)\right]^{(2+k_3)/2} \right\}^{2/(4+k_3)} \tag{8}$$

It should be noted that $k_2 > 0$ and $k_3 < 0$. Furthermore, in general, $|k_3| < 1$; thus, all exponents in Eq. (8) are positive.

The corresponding lift coefficient of the maximum lift-to-drag ratio, $\tilde{C}_L$, is

$$\tilde{C}_L = \left[\frac{k_2}{k_1}\left(\frac{1}{\nu}\sqrt{\frac{2W}{\rho}}\right)^{k_3} (1 - k_4)\right]^{1/(2-k_4)} \mathrm{AR}^{(1+k_4)/(2-k_4)} \tag{9}$$

The most significant implication of Eq. (8) is that the maximum lift-to-drag ratio grows limitless with the aspect ratio. This conclusion is in disagreement with the results shown in Fig. 1. Although the rate at which the maximum lift-to-drag ratio increases becomes less at large aspect ratios, it nevertheless keeps increasing, as the example for a wing with a NACA 0009 airfoil shows in Fig. 5. Further findings of Eq. (8) are the proportionality of the maximum lift-to-drag ratio to span efficiency and aircraft weight. The latter is directly related to the chord Reynolds number of the wing.

Minimum Power Required

The condition for the minimum power required can be determined using a similar analytical approach, as was done for the maximum lift-to-drag ratio. Using Eq. (6), the power required of a wing depends, in part, on the following nondimensional function of the lift coefficient and the aspect ratio:

$$\frac{C_L^{1.5}}{C_D} = \frac{\mathrm{AR}}{C_L^{1/2}\{k_1 + k_2 [(1/\nu)\sqrt{(2W/\rho)}]^{k_3} \mathrm{AR}^{k_4 - 1} C_L^{k_4 - 2}\}} \tag{10}$$

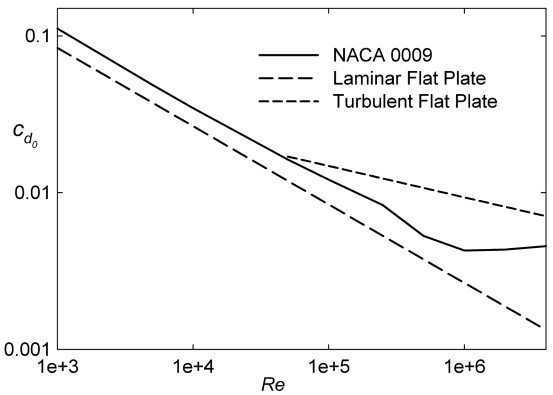

Fig. 4 Minimum drag coefficients as functions of the Reynolds numbers of a flat plate with laminar and turbulent boundary layers as well as of a NACA 0009.

The minimum of the power required yields

$$\left(\frac{C_L^{1.5}}{C_D}\right)_{\max} = \frac{\mathrm{AR}^{(3/2)[(1-k_4)/(2-k_4)]}}{\{(k_2/k_1)[(1/\nu)\sqrt{2W/\rho}]^{k_3}\}^{1/(4-2k_4)}(k_1 + k_2[(1/\nu)\sqrt{2W/\rho}]^{k_3}\{(k_2/k_1)[(1/\nu)\sqrt{2W/\rho}]^{k_3}\}^{(k_4-1)/(2-k_4)}\mathrm{AR}^{-2})} \tag{11}$$

The corresponding lift coefficient, $\hat{C}_L$, is:

$$\hat{C}_L = \left(\frac{k_5}{k_1}\right)^{1/(2-k_4)} \mathrm{AR}^{(1+k_4)/(2-k_4)} \tag{12}$$

It is noteworthy that the lift coefficient of minimum power required is larger by the factor of $[1/(1-k_4)]^{1/(2-k_4)}$ than the lift coefficient of the maximum lift-to-drag ratio of Eq. (9). For the example, when employing the NACA 0009 airfoil, the minimum power lift coefficient is 16% greater than the one of the maximum lift-to-drag ratio.

On inspection of Eq. (11), it becomes clear that the inverse of the minimum power required increases proportional with the aspect ratio. An example of the behavior of Eq. (11) is also plotted in Fig. 5. Similar to the maximum lift-to-drag ratio, the ratio of $C_L^{1.5}/C_D$ keeps increasing with the aspect ratio, although the rate of increase decreases significantly for aspect ratios larger than three.

Limitations of the Analytical Approach

The analytical approach has certain limitations that might lead to the incorrect conclusion that an infinite aspect ratio represents the optimum when concerned about flight performance. For example, stall clearly sets a limit to the growth of the optimal lift coefficient in Fig. 5. In fact, the maximal attainable lift coefficient usually decreases with decreasing Reynolds numbers. In general, the analytical approach disregards the viscous effects that become increasingly influential with the decrease in chord Reynolds numbers of the higher aspect ratios. In addition to the stall limit, nonlinear drag behaviors, such as the sudden drag increase at angles of attack that are beyond the low drag regions of an airfoil, are limitations that are not captured by the analytical approach. Consequently, nonlinear drag behavior and stall invalidate the logarithmic relationship assumption of Eq. (2) at larger aspect ratios and the corresponding lower chord Reynolds numbers. In contrast to the prediction of the analytical approach, one can expect that airfoil stall and the overproportional profile-drag increase result in the eventual deterioration of the performance, as the chord Reynolds number decreases as the aspect ratio increases for a constant wing area. To better evaluate these effects, a more comprehensive approach is needed.

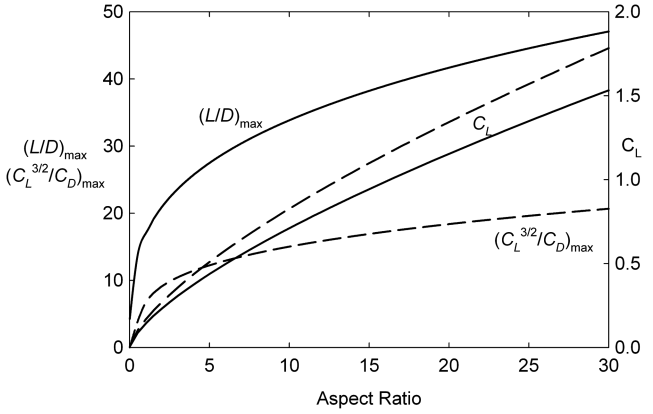

Fig. 5 Maximum lift-to-drag ratio of Eq. (8) and maximum $C_L^{1.5}/C_D$ of Eq. (11), as well as respective lift coefficients of Eqs. (9) and (12) versus aspect ratio. The aircraft mass is 100 g, and the wing has a NACA 0009 airfoil and a span efficiency of $e = 0.9$. Otherwise, standard sea-level conditions are assumed.

Quantitative Evaluation of the Optimal Aspect Ratio

In addition to the analytical approach, a computational study was used to investigate the optimal aspect ratio of rectangular wings. Of particular interest is the aerodynamic performance with respect to varying aspect ratios of a constant wing area in order to explore the tradeoff between induced and profile drags. Furthermore, the influence of different Reynolds number ranges is investigated using a number of wing area and mass combinations. Before the results of the aspect-ratio study are discussed, the computational method is introduced, and comparisons with experimental data are shown to demonstrate the validity of the prediction. In addition, other influential effects are explored using the computational method, such as the choice of airfoil.

Drag Decomposition

The computational method used for the quantitative optimal aspect-ratio study determines and adds the individual drag contributions. The individual drag contributions include induced drag, profile drag, and drag due to side-edge separation. The latter is primarily a concern for very low aspect-ratio wings and includes a lift correction. Drag decompositions generally exhibit good agreements with experimental results of low-speed flight, for example, for the design of winglets of high-performance sailplanes [12].

In the approach used herein, the induced drag is determined using an advanced potential flow method that models the lifting surface and the wake using elements with distributed vorticity [13]. The continuous and relaxed wake-vortex sheet is developed using a time-stepping method until the change in span efficiency is less than a predetermined value between two time steps. Besides determining the induced drag, the potential flow method is also used to determine the spanwise lift distribution. The total lift and induced drag are corrected for the additional lift due the side-edge separation.

Based on the spanwise lift distribution and the corresponding chord Reynolds numbers, the profile drag is determined at several spanwise stations using theoretical two-dimensional airfoil-drag data. The two-dimensional drag data were generated using XFOIL, as shown, for example, in Fig. 6. Although some of the boundary-layer assumptions made for XFOIL have limited validity for very low Reynolds numbers, such as zero-pressure gradients perpendicular to the flow in the boundary layer, the computational results using a program similar to XFOIL and an incompressible Navier–Stokes method agree reasonably well for airfoils operated at chord Reynolds numbers as low as 1000 [14].

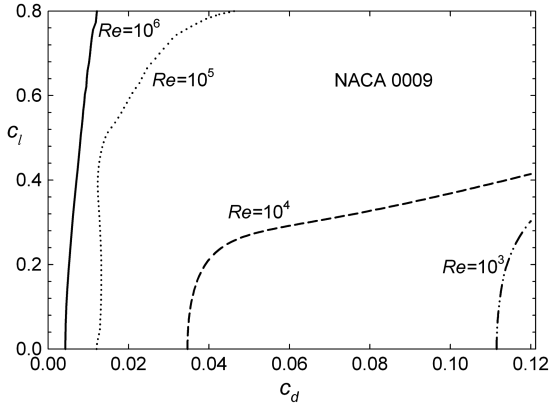

Fig. 6 Theoretical drag coefficients of the NACA 0009 airfoil at various Reynolds numbers [11].

As mentioned, the additional lift and drag due to flow around the side edges of the wing are considered, which is mainly an issue for wings of very small aspect ratios near unity and at high angles of attack. The lift and drag effects associated with the separated flow around the side edges are estimated using a curve fit of the tip suction force coefficient of [8]:

$$K_{v,se} = 2.95\mathrm{e}^{-0.3063\mathrm{AR}} \tag{13}$$

The subsequent lift-coefficient and drag-coefficient increments are

$$\Delta C_{L,se} = K_{v,se}\sin^2(\alpha)\cos(\alpha) \tag{14a}$$

and

$$C_{D,se} = K_{v,se}\sin^3(\alpha) \tag{14b}$$

Full leading-edge suction was assumed for the drag decomposition, since its influence on the maximum lift-to-drag ratio and minimum power required is negligible due to the large drag increase associated with the leading-edge separation. Nevertheless, leading-edge and side-edge separations can have significant impacts on the maximum lift produced, especially at low Reynolds numbers, thus having an influence on the minimum possible flight speed and the required wing area.

Comparison with Experimental Results

Comparisons of the drags of a low aspect-ratio wing that were obtained in wind-tunnel experiments [15,16] and using the described drag-decomposition method are shown in Fig. 7. Good agreement exists for most of the lift-coefficient range and in the predicted lift-to-drag ratios and nondimensional power-required points. Furthermore, the drag decomposition and the experiment predict similar lift coefficients at which the performance measures peak.

To assess the reliability of the computational method at higher aspect ratios, theoretical and experimental performance results of a small UAV with an aspect ratio of nearly 19 are shown in Fig. 8. The results are for the entire aircraft, including the fuselage, the empennage, and any interference-drag contribution. The decomposed drags of the computational results are plotted in Fig. 3. For a large part of the lift-coefficient range, good agreement exists, although the computational results are more optimistic, especially for the lower lift coefficients. These differences are very likely related to the larger scatter of the experimental data, especially at higher speeds. Another potential source of error is the theoretical airfoil drag that was generated using XFOIL and may be too optimistic. Such an error would matter particularly strongly at lower lift coefficients, where profile drag dominates.

In summary, the drag-decomposition method provides reliable theoretical drag data for low and high aspect-ratio wings in order to investigate aspect-ratio effects on the overall aerodynamic performance of wings. The computational approach sufficiently and accurately predicts the optimal performance values: that is, the maximum lift-to-drag ratio and the nondimensional minimum power-required point. In comparison with the experiments, the prediction also appears to predict the lift coefficients that correspond with the optimal performance values quite well.

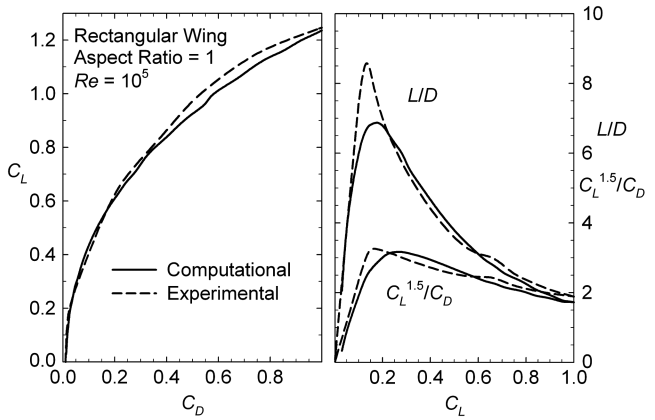

Fig. 7 Comparisons between experimental [15] and theoretical results of a wing with an aspect ratio of one and a flat-plate airfoil.

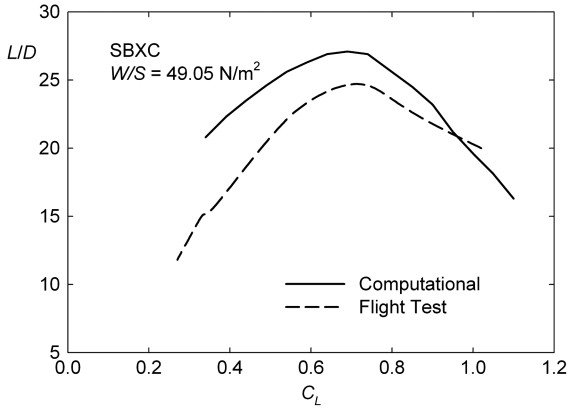

Fig. 8 Comparison between flight-test results and theoretical predictions of a model glider with an aspect ratio of approximately 19. (Data available online at http://xcsoaring.com/techPicts/Edwards%20performance%20test.pdf [retrieved 24 July 2009].)

Aspect-Ratio Study

The performances of the rectangular wings of different aspect ratios and weights were investigated using the drag-decomposition method explained previously. For the advanced potential flow code, each wing was modeled using 40 elements across the span and four along the chord. In the streamwise direction, the elements in the wake measured a quarter of the wing chord. The relaxed wake was developed using a time-stepping approach until the change in the span-efficiency factor was less than 0.005. The profile drags were interpolated for the appropriate lift coefficients and the Reynolds numbers, using theoretical section drags of an NACA 0009 airfoil.

Several different weight configurations were investigated. Although it initially seems to be at odds with the conventional understanding of the maximum flight performance depending on wing loading, the herein-discussed optimum performance values depend solely on weight and the aspect ratio. This seeming disagreement is easily explained with the fact that the conventional approach varies the wing loading by altering the weight and maintaining a given wing area. A heavier flight weight results in better performance due to the higher flight speeds for a given lift coefficient that lead to higher Reynolds numbers and subsequent lower profile-drag coefficients. For the herein-presented results, the induced drag and the corresponding spanwise and overall lift coefficients were determined using potential flow, which solely depends on the angle of attack and the wing aspect ratio. Any subsequent performance differences are due to profile-drag variations that result from differences in Reynolds numbers. Upon revisiting Eq. (3), it can be seen that the Reynolds number depends on the square root of weight divided by the aspect ratio and the lift coefficient. Consequently, the Reynolds number and subsequent profile-drag coefficient remain unchanged when varying the wing loading by changing the wing area while keeping the weight and the aspect ratio constant. Conversely, for a fixed aspect ratio and wing loading, the Reynolds number is a function of the weight. Nevertheless, one has to bear in mind that, despite the nondimensional performance parameter $C_L^{1.5}/C_D$ being independent of wing loading, the required power does depend on wing loading in addition to weight. Hence, the herein-presented results identify the optimal aspect ratios of a given weight and wing area.

For each wing-weight and aspect-ratio configuration, the drag polar was computed over an angle of attack range from 2 to 10 deg and in 0.1 deg increments. Based on these theoretical results, the maximum lift-to-drag ratio and minimum nondimensional power-required coefficient, as well as the corresponding lift

coefficients, were determined for each drag polar. The subsequent results of the maximum performance values of each wing configuration are plotted in Fig. 9. In particular, the lighter configurations and their lower chord Reynolds number ranges display distinct maxima in the flight performance with respect to the aspect ratio. With increasing flight weight, the optimal aspect ratios move to larger peak values and eventually plateau without displaying a distinct maximum value. Some waviness is visible in the computed data, especially in the lift-coefficient results. This waviness is primarily due to nonlinearities introduced by the relaxed wake. In general, the lift coefficients peak at similar aspect ratios as the performance values.

Although the analytical investigation summarized in Fig. 5 gives some insight in the behavior of the optimal performance parameters and their corresponding lift coefficients, little agreement exists with the computational results of the 100 g wing in Fig. 9. The analytical result clearly overpredicts performance and corresponding lift coefficients, even at aspect ratios that are less than the computational optimal one. The optimistic analytical results are a reflection of the nonlogarithmic behavior of the profile drag, as it is assumed to be logarithmic in the analytical investigation.

The computed higher performance of the heavier wings is a direct result of the different Reynolds number ranges that each wing operates. This is illustrated well in Figs. 10 and 11 that show the aspect-ratio dependency of Reynolds number and the individual drag contributions of the minimum nondimensional power-required coefficients of the 500 g and 5 kg wing, respectively. The graphs have been smoothed slightly by merely using selected aspect ratios. The induced drags and the drags associated with the side-edge vorticity behave fairly similar with the aspect ratio, as one would expect from the potential solution at equal aspect ratios and similar lift coefficients. In contrast with that, however, the profile drag of the lighter wing is considerably larger than for the heavier wing at the same aspect ratio. The larger profile drag of the 500 g wing is directly related to its lower Reynolds numbers that are nearly one third of the values of the heavier wing at the same aspect ratio. At the optimal aspect ratios of the 500 g wing, 16, the Reynolds numbers differ by a factor of nearly three. The subsequent profile drags differ by nearly 50%. Even at the optimal aspect ratio of the 5 kg wing, approximately 20, the differences are similarly in favor of the heavier wing. The performance advantage of the heavier wing due to Reynolds number effects is compounded by its smaller induced drag at the larger aspect ratio. It can be concluded that the higher Reynolds numbers, at which the heavier wing operates, move the optimal solution to higher aspect ratios, giving this wing the advantage of the higher aspect ratio.

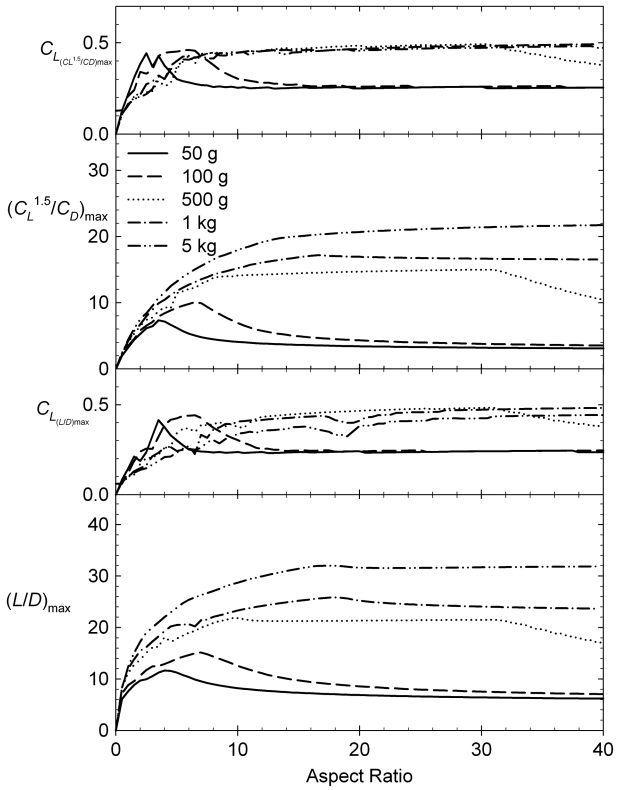

Fig. 9 Maximum lift-to-drag and minimum power-required values with respect to the aspect ratio of rectangular wings of different flight weights.

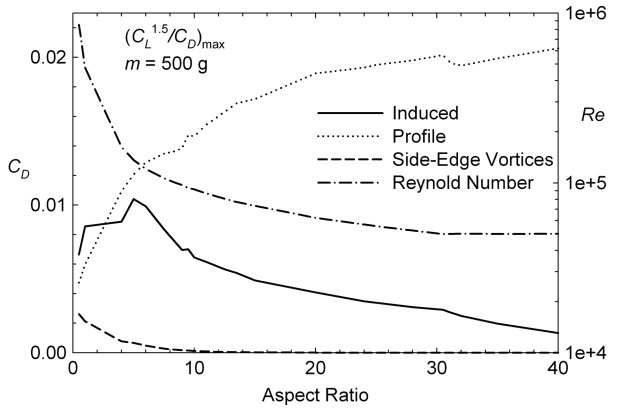

Fig. 10 Individual drag contributions and the chord Reynolds number of the minimum power-required point of the 500 g wing with varying aspect ratios.

Other Parameters Impacting the Optimal Aspect Ratio

Further parameters also have an influence on the magnitude of the optimal aspect ratio and the respective lift coefficient. Examples of such parameters are the addition of a fuselage, the need for stable and controlled flight, as well as the choice of airfoil. Beyond those issues, other requirements might drive the choice of aspect ratio, such as a limited span due to operational requirements and/or the need for sufficient wing area for slow-flight capabilities.

Any additional parasitic drag generally reduces the maximum performance values and favors smaller optimal aspect ratios. In that respect, the presence of the fuselage is detrimental from a purely aerodynamic point of view, although it is still needed for other purposes. Similarly, a lower aspect-ratio wing is likely to have a greater trim drag than its higher aspect-ratio counterpart of an equivalent wing area, since the former is likely to require a larger horizontal tail for longitudinal stability. The disadvantage of the larger horizontal tail surface might, however, be counterbalanced by a reduced vertical-tail area if constant tail volumes are maintained. An example of the detrimental effect of the horizontal tail and fuselage is given with the small UAV for which the theoretical drag components are shown in Fig. 3. As shown in Fig. 8, the maximum lift-to-drag ratio of the entire aircraft is approximately 27. In contrast

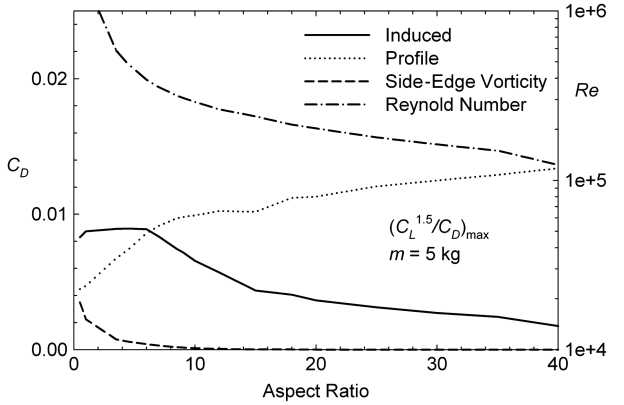

Fig. 11 Individual drag contributions and the chord Reynolds number of the minimum power-required point of the 5 kg wing with varying aspect ratios.

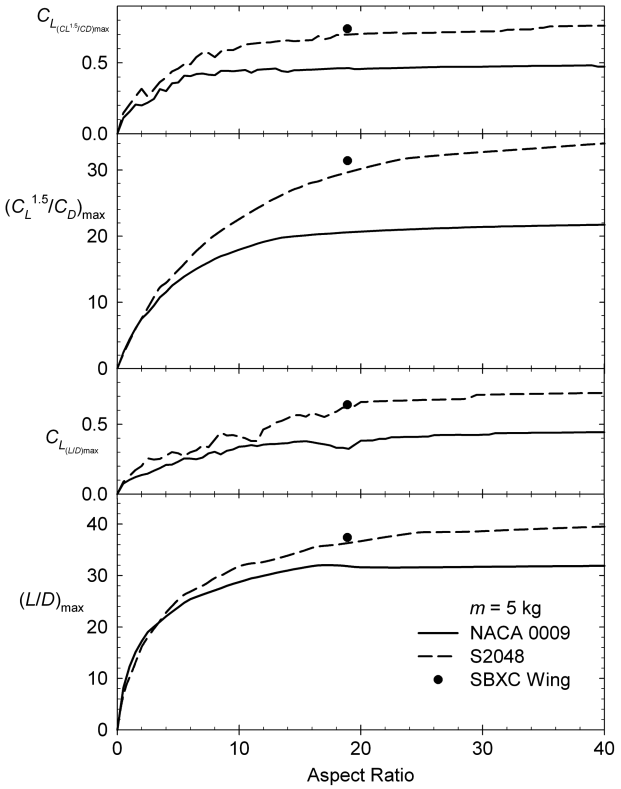

Fig. 12 Airfoil effects on the maximum lift-to-drag and minimum power-required values for rectangular wings of 5 kg mass and with varying aspect ratios.

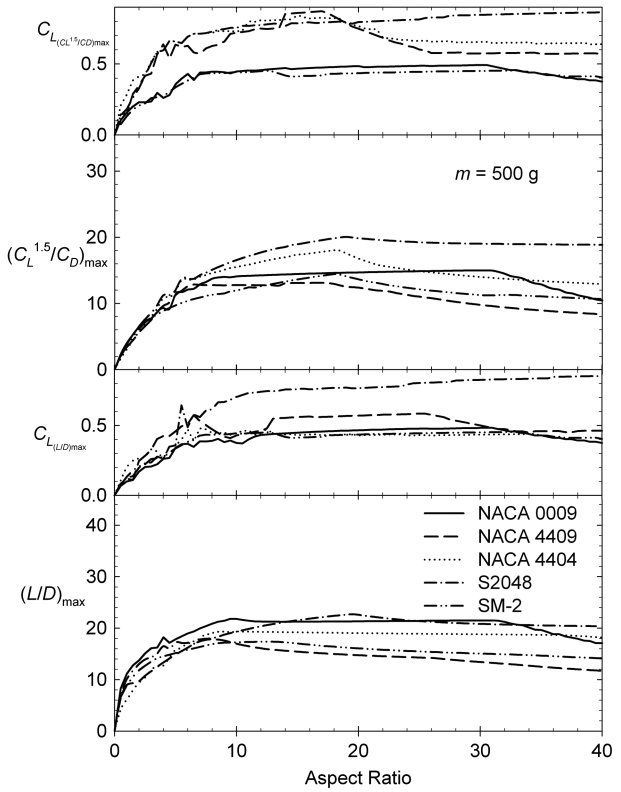

Fig. 13 Thickness and camber effects on the maximum lift-to-drag and minimum power-required values for rectangular wings of 500 g mass and with varying aspect ratios.

with that, the theoretical maximum lift-to-drag ratio of the isolated wing is roughly 10 points higher, as indicated by the solid dots in Fig. 12. A similar performance increase applies to the minimum power-required condition; although, in this case, the higher span efficiency of the SBXC wing results in a slight advantage over the rectangular wing planform.

The effect of different airfoils is investigated in Figs. 12 and 13. In Fig. 12, the maximum performance parameters are shown of the 5 kg wing with varying aspect ratios. The influence of two different airfoils was investigated using the symmetrical NACA 0009 airfoil and the S2048 airfoil. The latter airfoil has an approximately 2% camber and a maximum relative thickness of 8.6% [17]. As one would expect, the use of an airfoil designed for that flight regime, the S2048, does improve the maximum performance parameters and moves the corresponding lift coefficients to higher values. Less clear is the advantage of airfoil choice for the lighter wing of 500 g, as shown in Fig. 13. In addition to the previously mentioned airfoils, the case of the 6% thick airfoil that has been used on other MAV designs was included in this figure. The characteristics of this airfoil are taken from [18]. The various airfoils have only a limited influence on the maximum lift-to-drag ratio, whereas, depending on the airfoil, slight improvements are visible for the nondimensional minimum power-required points. Just as in the 5-kg-wing case, the increase of airfoil curvature moves the lift coefficients that correspond to the performance maxima to higher values. It can be concluded that the increase of this performance parameter is primarily due to the cambered airfoil having a low drag region at higher lift coefficients. If the higher lift, however, comes at the cost of significantly larger profile drags, as in the case of the 500 g wing, any significant performance may still be voided. Nevertheless, it remains to be seen if a properly designed airfoil can produce more significant advantages for either performance parameter.

The computational results are summarized in Fig. 14, in which are shown the dependency of the optimal aspect ratios on flight mass and the corresponding flight performances. To a limited extent, these figures can be used for initial sizing of aircraft of similar masses, especially for flight masses below 500 g. Such design examples are given in the next section. At these very low flight weights, the choice of airfoil appears to be of a lesser influence, at least in the cases of the airfoils used in this study. For heavier configurations, which have less pronounced maxima, the airfoil has a profound influence on the performance. These graphs, however, should not preclude that the influence of airfoil choice is negligible at the lower weights. Especially at the lower Reynolds numbers, the existence and bursting of laminar separation bubbles can result in certain airfoils being less adequate for a particular configuration. Nevertheless, the graphs are

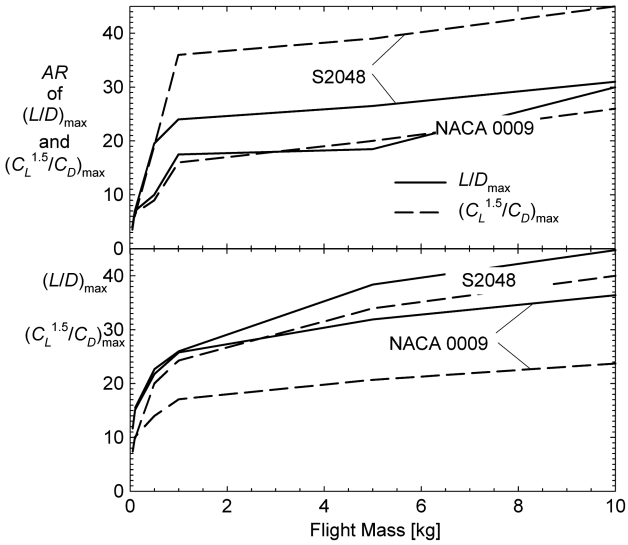

Fig. 14 Optimal aspect ratios and nondimensional maximum performance parameters' dependency on flight mass.

useful to identify general trends in the optimal aspect ratios that are helpful with initial design iterations.

Conceptual Design Examples Based on the Optimal Aspect Ratio

In this section, the optimal aspect-ratio quantification that is summarized in Fig. 14 is used for two conceptual design examples of small aerial vehicles. The first case is of a small UAV that has a flight mass of 2 kg, similar to hand-launched aircraft that are used for short-range reconnaissance. The second case is the study of a MAV of 100 g that has a 15-cm-span limitation for operational reasons. Either flight vehicle is propeller driven and has a reconnaissance mission; thus, it needs to be optimized for the minimum power required. Although it was not designed for these particular aircraft, the S2048 airfoil is chosen for either aircraft.

Two-Kilogram Unmanned Aerial Vehicle Design

UAVs of this weight category are typical for tactical UAVs that are often used for reconnaissance purposes by soldiers with very limited technical support. In general, the size of the wing area is driven by the need to hand launch such an aircraft. A minimum hand-launch velocity of approximately 18 kt appears to be plausible for that flight weight, which equates to a wing area of 0.37 m^2 when assuming a launch-lift coefficient of about one. Based on that weight and Fig. 14, the optimal aspect ratio for maximum endurance is 36. The subsequent wingspan is 3.65 m.

The predicted flight performance of the optimized aircraft is plotted in Fig. 15. The predicted maximum nondimensional minimum power-required coefficient of about 22 falls short of that listed in Fig. 14. Nevertheless, the theoretical maximum performance parameter is nearly twice the value of that of a smaller aspect-ratio aircraft that has an equivalent weight and wing area. The smaller spanned aircraft has dimensions that are more commonly used for this class of flight vehicles, such as the RQ-11 Raven of AeroVironment. The flight performance of either aircraft was performed using identical fuselages and tailbooms, as well as equivalent tail volumes and tail-aspect ratios.

Despite the, theoretically, almost double endurance of the optimal aspect ratio, the higher performance comes at a cost that, in the end, may favor the smaller spanned aircraft. Depending on the mission, the larger span might be impracticable due to operational constraints, such as transporting a wing with a span of 3.65 m in a backpack or hand launching such a winged aircraft under field conditions. In addition, the larger span results in significantly higher root-bending moments. The root-bending moment that, when assuming a constant spanwise lift distribution, is almost six times that of the smaller spanned UAV, requires a more substantial wing structure with the possible associated weight penalty. These structural concerns are exacerbated by the reduced maximum thickness of the smaller chord. Ultimately, the designer has to make the tradeoff decision of span versus operational and structural limitations.

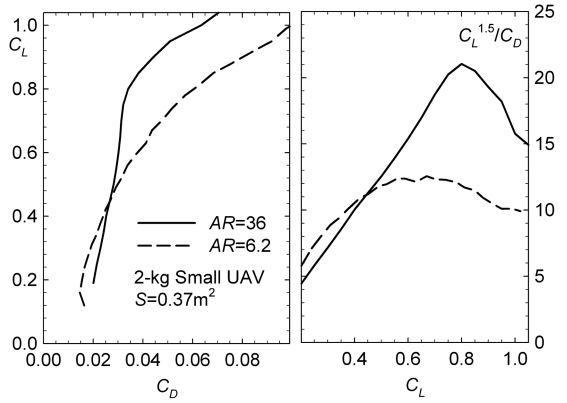

Fig. 15 Predicted flight performances of small UAVs with equal wing areas and flight weights but two different wing aspect ratios: one optimized in accordance with Fig. 14 and one of more common dimensions.

One-Hundred-Gram Micro Aerial Vehicle Design

MAVs have the potential to be used for reconnaissance missions in confined spaces, such as indoors or in wooded areas. Because of these operational constraints, the maximum dimensions of these flight vehicles are limited in order for them to navigate through doors, hallways, or between trees. Early MAV developments explored maximum spans of 15 cm and flight masses below 100 g, for example [18,19]. Many of these and similar designs maximize the wing area by using aspect ratios of two and less in order to reduce wing loading. Given that MAVs are generally designed for loiter missions and driven by a propeller system, a design aspect is their minimum power required in order to maximize their time on station. The power required depends on drag and flight speed:

$$P = DV_\infty = 1/2\rho V_\infty^3 S C_D \tag{15}$$

For limited wingspan and flight weight, the horizontal flight velocity in Eq. (15) can be replaced with the following relationship:

$$V_\infty = \sqrt{\frac{W}{1/2\rho C_L}\frac{b^2}{\mathrm{AR}}} \tag{16}$$

Hence, Eq. (15) yields

$$P = \frac{W^{3/2}}{b}\left(\frac{\mathrm{AR}}{1/2\rho}\right)^{1/2}\frac{C_D}{C_L^{1.5}} \tag{17}$$

On inspection of Eq. (17), it becomes apparent that the power required is proportional to the square root of the aspect ratio. In other words, while keeping everything else constant, doubling the aspect-ratio results in roughly 40% more power required. This greater need for power to sustain horizontal flight is due to the necessity of a larger flight speed in order to compensate for the smaller wing area that has been halved in order to double the aspect ratio and maintain the wingspan. From Eq. (17), however, one can also deduce that the power required is inversely proportional to the nondimensional power-required coefficient, $C_L^{1.5}/C_D$. Indeed, when considering the predicted minimum power coefficients, $C_L^{1.5}/C_D$, for different aspect ratios of Fig. 9, the low points of the minimum power required become evident for aspect ratios ranging from about 2.0 to 6.5, as apparent in Fig. 16. For these aspect ratios, an approximate 20% increase in endurance seems achievable in comparison to an aspect ratio of 1.0. Although not necessarily a prime design aspect, increasing the aspect ratio from 1 to 6.5 also bears the benefit of nearly doubling the possible range. Nevertheless, from an operational standpoint, the lower aspect ratio of 2.0 might be preferable despite the lesser range of the aspect ratio of 6.5. A mission in

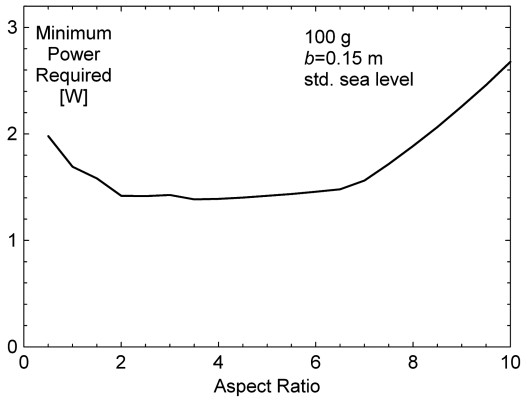

Fig. 16 Minimum power required for a 100 g MAV with a 15-cm-wingspan restriction.

confined spaces using the higher aspect-ratio wing may not be practical due higher flight speed of the smaller wing area.

Conclusions

An analytical analysis that uses a power-law approximation for the minimum profile drag does not support the notion of an optimal aspect ratio that maximizes the flight performance. In fact, the analysis shows no limit to the maximum performance parameters as the aspect ratio is increased. This unlimited behavior is due to the analytical approach not capturing nonlinear effects, such as stall. Although the theory promotes infinitely large aspect ratios for maximum aerodynamic performance, the viscous reality suggests much more finite spans as optimal solutions.

A more comprehensive answer to the question of the optimal aspect ratio is found using a computational approach that employs a drag-decomposition scheme, which considers induced, vortical, and viscous effects. The computational results show that, in order to maximize the aerodynamic performance parameters, heavier configurations favor higher aspect ratios than the lighter wings. In addition, whereas the very light configurations of 50 and 100 g have distinct maxima for their aerodynamic performance as the aspect ratio is varied, the higher mass wings of 1 and 5 kg display performance plateaus that last up to and beyond the investigated maximum aspect ratio of 40. These differences in maximum aerodynamic performance are directly related to the operational Reynolds number ranges of each weight configuration.

The computational analysis indicates that, particularly, lighter flight weights benefit from aspect ratios that differ significantly from unity, as favored by many recent studies. The advantage of the higher aspect ratio is exemplified with the nondimensional parameter for maximum endurance of propeller aircraft. For example, based on the herein-discussed results for a 100 g vehicle with a 15 cm wingspan restriction, increasing the aspect ratio from 1 to 2.0 has the potential of increasing the endurance by 20%. A further increase to an aspect ratio of 6.5 also doubles the potential range of the aircraft. Unlike for larger aircraft, it can be expected that this significant performance gain should come at no or only little extra structural weight penalty. Thus, despite other limiting design aspects, already modest increases in aspect ratio can lead to significant flight performance improvements in the case of small vehicles and MAVs and should be fully considered by the designer.

A remaining source of inaccuracy in the computational study is that most of the airfoils used in this study were designed for Reynolds number ranges that were well above the ones needed for this study. Especially at Reynolds numbers below 100,000, laminar separation bubbles caused highly nonlinear behaviors in the airfoil characteristics. Undoubtedly, properly designed airfoils can greatly affect the performance of an aircraft, even of the smaller scale. At the lower Reynolds numbers that are typical for small vehicles and MAVs, only a very limited amount of experimental and theoretical airfoil data exist. Thus, more experimental data at low and very low Reynolds numbers are desirable for the design of small vehicles and MAVs, as well as the development and validation of theoretical methods.

Acknowledgments

Special thanks for valuable input and discussions belongs to Mark Maughmer and David Maniaici, both of Penn State University, as well as to Mike Baur of the Naval Research Laboratory.

References

[1] Spedding, G. R., and Lissaman, P. B. S., "Technical Aspects of Microscale Flight Systems," *Journal of Avian Biology*, Vol. 29, No. 4, 1998, pp. 458–468.

[2] Cosyn, P., and Vierendeels, J., "Design of Fixed Wing Micro Air Vehicles," *Aeronautical Journal*, Vol. 111, No. 1119, May 2007, pp. 315–326.

[3] Viieru, D., Albertini, R., Shyy, W., and Ifju, P. G., "Effect of Tip Vortex on Wing Aerodynamics of Micro Air Vehicles," *Journal of Aircraft*, Vol. 42, No. 6, Nov.–Dec. 2005, pp. 1530–1536. doi:10.2514/1.12805

[4] Null, W., and Shkarayev, S., "Effect of Camber on Aerodynamics of Adaptive-Wing Micro Air Vehicles," *Journal of Aircraft*, Vol. 42, No. 6, Nov.–Dec. 2005, pp. 1537–1542. doi:10.2514/1.12401

[5] Ramamurti, R., and Sandberg, W., "Computation of Aerodynamic Characteristics of a Micro Air Vehicle," *Fixed and Flapping Wing Aerodynamics for Micro Air Vehicle Applications*, edited by T. J. Mueller, Progress in Astronautics and Aeronautics, AIAA, Reston, VA, 2001, pp. 537–555.

[6] Polhamus, E. C., "A Concept of the Vortex Lift of Sharp-Edge Wings Based on a Leading-Edge-Suction Analogy," NASA TN D-3767, 1966.

[7] Polhamus, E. C., "Predictions of Vortex-Lift Characteristics by Leading-Edge Suction Analogy," *Journal of Aircraft*, Vol. 8, No. 4, April 1971, pp. 193–199. doi:10.2514/3.44254

[8] Lamar, J. E., "Extension of Leading-Edge-Suction Analogy to Wings with Separated Flow around the Side Edges at Subsonic Speeds," NASA TR 428, Oct. 1974.

[9] Anderson, J. D., *Introduction to Flight*, 6th ed., McGraw–Hill, New York, 2008.

[10] Pamadi, B. N., *Performance, Stability, and Control of Airplanes*, 2nd ed., AIAA Education Series, AIAA, Reston, VA, 2004.

[11] Drela, M., "XFOIL: An Analysis and Design System for low Reynolds Number Airfoil," *Proceedings of the Conference on Low Reynolds Number Aerodynamics*, edited by T. Mueller, Springer–Verlag, Berlin, 1989, pp. 1–12.

[12] Maughmer, M. D., "Design of Winglets for High-Performance Sailplanes," *Journal of Aircraft*, Vol. 40, No. 6, Nov.–Dec. 2003, pp. 1099–1106. doi:10.2514/2.7220

[13] Bramesfeld, G., and Maughmer, M. D., "A Relaxed Wake Vortex-Lattice Method Using Distributed Vorticity Elements," *Journal of Aircraft*, Vol. 45, No. 2, March–April 2008, pp. 560–568. doi:10.2514/1.31665

[14] Kunz, P. J., and Kroo, I., "Analysis and Design of Airfoils for Use at Ultra-Low Reynolds Numbers," *Fixed and Flapping Wing Aerodynamics for Micro Air Vehicle Applications*, edited by T. J. Mueller, Progress in Astronautics and Aeronautics, AIAA, Reston, VA, 2001, pp. 35–60.

[15] Torres, G. E., "Aerodynamics of Low Aspect Ratio Wings at Low Reynolds Numbers With Application to Micro Air Vehicle Design," Ph.D. Thesis, Univ. of Notre Dame, Notre Dame, IN, April 2002.

[16] Torres, G. E., and Mueller, T. J., "Aerodynamics of Low Aspect Ratio Wings," *Fixed and Flapping Wing Aerodynamics for Micro Air Vehicle Applications*, edited by T. J. Mueller, Progress in Astronautics and Aeronautics, AIAA, Reston, VA, 2001, pp. 115–141.

[17] Selig, M. S., Donovan, J. F., and Fraser, D. B., *Airfoils at Low Speeds*, edited by H. A. Stokely, Soartech 8, Virginia Beach, VA, 1989.

[18] Kellogg, J. C., "Case Study: Micro Tactical Expendable Rigid-Wing Micro Air Vehicle," *Introduction to the Design of Fixed-Wing Micro Air Vehicles*, AIAA Education Series, AIAA, Reston, VA, 2006, pp. 151–184.

[19] Cosyn, P., and Vierendeels, J., "Design of Fixed Wing Micro Air Vehicles," 20th Bristol UAV Systems Conference, Univ. of Bristol Paper 25, Bristol, U. K., April 2005.